Biosensors and Bioelectronics 107 (2018) 203–210

Contents lists available at ScienceDirect

Biosensors and Bioelectronics

journal homepage: www.elsevier.com/locate/bios

Theoretical and experimental study for the biomimetic recognition of levothyroxine hormone on magnetic molecularly imprinted polymer

Silio Lima Moura[a,1], Laura Martinez Fajardo[a,1], Leonardo dos Anjos Cunha[b], Maria Del Pilar Taboada Sotomayor[c], Francisco Bolivar Correto Machado[b], Luiz Fernando Araújo Ferrão[b,*], Maria Isabel Pividori[a,*]

[a] Grup de Sensors i Biosensors, Departament de Química, Universitat Autònoma de Barcelona, 08193 Bellaterra, Spain
[b] Instituto Tecnológico de Aeronáutica, Departamento de Química, São José dos Campos, 12228-900 São Paulo, Brazil
[c] Instituto de Química, Departmento de Química Analítica, Universidade Estadual de São Paulo (UNESP), 14801-970 Araraquara, São Paulo, Brazil

ARTICLE INFO

Keywords:
L-thyroxine
Magnetic-MIP
Rational MIP design
Electrochemical sensing
Magnetic actuation

ABSTRACT

This study addresses the rational design of a magnetic molecularly imprinted polymer (magnetic-MIP) for the selective recognition of the hormone levothyroxine. The theoretical study was carried out by the density functional theory (DFT) computations considering dispersion interaction energies, and using the D2 Grimme's correction. The B97-D/def2-SV(P)/PCM method is used not only for studying the structure of the template the and monomer-monomer interactions, but also to assess the stoichiometry, noncovalent binding energies, solvation effects and thermodynamics properties such as binding energy. Among the 13 monomers studied *in silico*, itaconic acid is the most suitable according to the thermodynamic values. In order to assess the efficiency of the computational study, three different magnetic-MIPs based on itaconic acid, acrylic acid and acrylamide were synthesized and experimentally compared. The theoretical results are in agreement with experimental binding studies based on laser confocal microscopy, magneto-actuated immunoassay and electrochemical sensing. Furthermore, and for the first time, the direct electrochemical sensing of L-thyroxine preconcentrated on magnetic-MIP was successfully performed on magneto-actuated electrodes within 30 min with a limit of detection of as low as 0.0356 ng mL^{-1} which cover the clinical range of total L-thyroxine. Finally, the main analytical features were compared with the gold standard method based on commercial competitive immunoassays. This work provides a thoughtful strategy for magnetic molecularly imprinted polymer design, synthesis and application, opening new perspectives in the integration of these materials in magneto-actuated approaches for replacing specific antibodies in biosensors and microfluidic devices.

1. Introduction

The levothyroxine (3,5,3′,5′-tetraiodothyronine), also known as L-thyroxine or T4, is an essential hormone produced in the human thyroid gland which causes abnormality in the metabolism when its concentration in the blood-stream is unbalanced (Gentile et al., 1995). In this context, the L-thyroxine, as well as the thyroid-stimulating hormone (TSH), are considered the most important biomarkers for the screening of thyroid disorders (Dayan, 2001). The gold standard serologic tests for the detection of L-thyroxine are based on competitive immunoassay using specific antibodies against the hormone (Midgley, 2001). Molecularly imprinted polymers (MIPs) are synthetic biomimetic materials mimicking biological receptors (Vlatakis et al., 1993). They are highly cross-linked macromolecular structures towards the template which is then extracted after polymerization, originating cavities (binding sites) complementary to the template molecule, acting similarly as plastic antibodies. The MIP technology is based on non-covalent interactions between the polymer and the template to recognize its unique pattern. Although MIPs show in general lower affinity and selectivity compared to the biological counterparts, they present remarkable technological features: (i) they can be easily synthesized on animal-free large-scale procedures, and (ii) they show high chemical and mechanical stability, allowing to work in harsh conditions (Ben Aissa et al., 2016). The integration of MIPs were widely reported for a huge range of target molecules in different approaches including biosensors (Jolly et al., 2016), immunoassays (Wang et al., 2015),

* Corresponding authors.
E-mail addresses: ferrao@ita.br (L.F. Ferrão), isabel.pividori@uab.cat (M.I. Pividori).
[1] These authors contributed equally to this work.

https://doi.org/10.1016/j.bios.2018.01.028
Received 10 November 2017; Received in revised form 9 January 2018; Accepted 13 January 2018
Available online 31 January 2018
0956-5663/

electronic tongues (Huynh and Kutner, 2015), among many others. Furthermore, the synergic association with other materials including quantum dots (Ren and Chen, 2015), graphene (Zeng et al., 2013), and lately, magnetic particles (Ben Aissa et al., 2016) were also recently reported. The ligand-receptor interaction is the main feature in determining both the affinity and the selectivity of a MIP, which mainly depends on the choice of a suitable functional monomer. Many researchers based this selection by synthesizing several MIPs with different monomers followed by further laboratory testing. However, this is a costly approach, which can be speed up with the aid of computational simulations, such as combinatorial chemistry (Mahon and Fulton, 2014), chemometrics (Rosengren et al., 2009) and molecular mechanics (Nicholls et al., 2009). Among them, quantum chemistry within several methodologies such as density functional theory (DFT) is considered reliable approach for study of ligand-receptor interactions (Bhaskarapillai et al., 2009). However, the dispersion forces (such as van der Waals interactions), which affect the arrangement of an organic ligand towards a target molecule (template) are not accounted by the standard DFT methods, leading to non-accurate molecular geometries and systematic errors. Dispersion-corrected DFT (DFT-D) approach, which consists in including a semi-empirical long-range dispersion correction to the conventional Kohn-Sham DFT energy, provides significant improvements in the accuracy with reasonable computational cost (Řezáč and Hobza, 2016).

This work addresses a rational MIP design based on the DFT-D quantum chemistry calculations among different functional monomers for the noncovalent recognition of L-thyroxine as a template. In order to assess the predictive efficiency of DFT-D approach, three different magnetic-MIPs were synthesized based on different monomers and experimentally tested by magneto-actuated immunoassay, laser confocal microscopy and electrochemical sensing. The magnetic-MIP based on the itaconic acid showed outstanding binding capacity and limit of detection (LOD) for L-thyroxine, as predicted by the *in silico* DFT-D quantum chemistry calculations. This methodology presents promising features for the rational MIP design towards a variety of templates. To the best of our knowledge, this work describes, for the first time, DFT-D quantum chemistry calculations for the evaluation of the thermodynamic properties for the rational synthesis design, optimization as well as the synthesis and application of magnetic-MIP for an improved determination of L-thyroxine.

2. Materials and methods

2.1. Instrumentation

The SEM images were taken with MERLIN FE-SEM and Hitachi S-570. The TEM images were taken with JEM-2011. The confocal fluorescence images were taken with the TCP-SP5 Leica Microscope. Optical measurements were performed with an Infinite M200 PRO (TECAN) spectrophotometer. The electrochemical measurements were performed using an AUTOLAB PGSTAT10 electrochemical analyzer (Eco Chemie) using a m-GEC working electrode (Pividori and Alegret, 2005). Further details are provided in Supp. data.

2.2. Chemicals and biochemicals

The tracers T4-HRP and T4-Atto655 were synthesized as detailed described in Supp. Data (Schemes S1 and S2). L-thyroxine (No. T2376, Sigma Aldrich) and all other reagents were analytical grade (Supp. data). Ultrapure water (Millipore® System, resistivity 18.2 MΩ cm) was used throughout the experiments.

2.3. Theoretical calculations

All computations were performed with the Gaussian 9 (Frisch et al., 2013) computational package. The GGA functional B97-D (Grimme, 2006) which contains the D2 Grimme's dispersion correction was used for the geometry optimization of monomers and L-thyroxine ground state without symmetry constraints. This functional describes the dispersion interactions in organic ligands of biologically active compounds (Antony and Grimme, 2006). The basis set def2-SV(P) (Weigend et al., 2005) was used in all calculations. Effective core potentials (ECPs) (Hay and Wadt, 1985) of the Stuttgart–Dresden type were used for iodine atoms. Gaussian 09 default parameters were adopted for the numerical integration grids, self-consistent-field (SCF) and geometry optimization convergence criteria. The noncovalent binding energies of L-thyroxine with the different monomers were calculated at the same level of theory, followed by frequency computations to confirm the real minimum character of each optimized structures (no imaginary frequency at the stationary states).

The electronic binding energy (ΔE) (Eq. (1)) was calculated as the difference in electronic energy between the monomer/L-thyroxine complex ($E_{complex}$), interacting at a single configuration, compared to the non-interacting electronic energy of L-thyroxine ($E_{template}$) and monomers ($E_{monomer}$) at infinite separation. Long–range effects induced by different solvent polarity on the predicted thermodynamics properties, as ΔE, the Gibbs free energy ($\Delta G_{298.15\ K}$) and enthalpy ($\Delta H_{0\ K}$) (Eqs. (2) and (3)) were considered by means of a dielectric continuum approach using Tomasi's Polarizable Continuum Model (PCM) (Scalmani and Frisch, 2010). Explicitly solvent effects were also investigated.

$$\Delta E_{298.15K} = E_{complex} - E_{template} - \sum E_{monomer} \quad (1)$$

$$\Delta G_{298.15K} = (\varepsilon_0 + G_{corr})_{complex} - (\varepsilon_0 + G_{corr})_{template} - \sum (\varepsilon_0 + G_{corr})_{monomer} \quad (2)$$

$$\Delta H_{0K} = (\varepsilon_0 + H_{corr})_{complex} - (\varepsilon_0 + H_{corr})_{template} - \sum (\varepsilon_0 + H_{corr})_{monomer} \quad (3)$$

In the Eqs. (2) and (3), ε_0 is the total electronic energy, G_{corr} is the thermal free energy correction, H_{corr} is the enthalpy correction (zero-point energy).

Firstly, the calculations using DFT-D on monomers-template and monomer-monomer interactions, solvents and stoichiometry were carried out. The best conditions for the synthesis were considered for rational magnetic-MIP design for L-thyroxine.

2.4. Synthesis and characterization of the magnetic molecularly imprinted polymers for L-thyroxine

The magnetic-MIPs were synthesized using the procedure reported for synthesis of magnetic-MIPs (Ben Aissa et al., 2016) with slight modifications (schematically depicted in Fig. 1 and detailed described in Supp. data, Schemes S3–S5). The magnetic non-imprinted polymer (magnetic-NIP) (prepared without the template L-thyroxine) was used in all cases as a control to evaluate the specificity of the MIP-template interaction.

After each step of the core-shell synthesis, the product was collected and characterized by SEM and TEM, as detailed in Supp. data. Energy dispersive X-ray spectroscopy detector (EDS) was also used for the elemental analysis. Other characterization of the material during the synthesis was performed, including selected-area diffraction analysis (SAED), X-ray diffraction, UV spectrophotometry and FTIR.

2.5. Experimental evaluation of the performance of the magnetic-MIPs and magnetic-NIPs

2.5.1. Laser confocal microscopy

The binding patterns of L-thyroxine conjugated to Atto655 fluorophore (T4-Atto655) on magnetic-MIPs were performed by laser confocal microscopy (fluorescence emission at 680 nm). The magnetic-MIPs or magnetic-NIPs (0.55 mg) were incubated with T4-Atto665

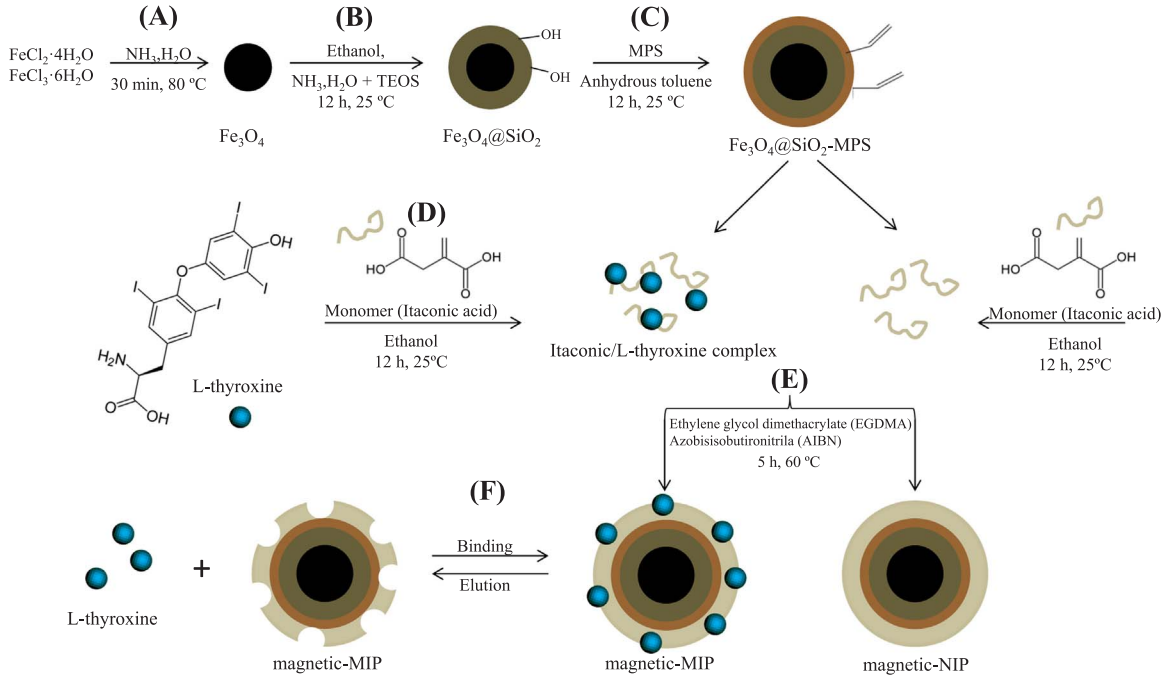

Fig. 1. Schematic representation of the synthesis of magnetic-MIPs and magnetic-NIPs for L-thyroxine. The synthesis is detailed described in Supp. Data.

conjugate 5.0 μmol L^{-1} in citrate buffer (pH 7.0) for 30 min with gentle shaking at 25 °C. Two washing steps were performed in citrate buffer (pH 7.0). The images were scanned using the laser AOTF at 633 nm excitation wavelength whereas the emission wavelength was captured at 680 nm. The schematic procedure is shown in Fig. S1 (Supp. data).

2.5.2. Magneto-actuated immunoassay

This procedure was performed to study the binding on magnetic-MIPs (and magnetic-NIPs) of L-thyroxine conjugated to enzyme horseradish peroxidase (T4-HRP), as schematically depicted in Fig. S2 and Video S1 (Supp. data). The magnetic-MIPs (0.55 mg) were placed in 96-well microtiter plates and incubated with 100 μL T4-HRP conjugate (ranging from 2.40 × 10^{-4} to 24.00 μg mL^{-1}) in citrate buffer (pH 7.0) for 30 min with gentle shaking at 25 °C, and a magnetic separator was used to remove the supernatant. After that, the 96-well plate was put over a magnetic separator (Video S1) to wash (3×) with 200 μL of citrate buffer (pH 7.0). The optical readout, was achieved by incubation with 100 μL of substrate solution (0.004% v/v H_2O_2 and 0.01% w/v 3,3′,5,5′-Tetramethylbenzidine (TMB) in citrate buffer) for 30 min at 25 °C under darkness. The enzymatic reaction was stopped by adding 100 μL of H_2SO_4 (2.0 mol L^{-1}). The absorbance measurement of the supernatant was thus performed with the microplate reader at 450 nm.

2.6. Electrochemical sensing on magneto-actuated electrodes

The direct electrochemical sensing of L-thyroxine was achieved for the first time by preconcentration on the magnetic-MIP with further magnetic actuation on the surface of m-GEC electrode, as schematically shown in Fig. 2 and Video S2 (Supp. data). The amount of magnetic-MIP (from 0.10, 0.55 and 1.00 mg) was optimized by SEM in order to evaluate the distribution of the magnetic-MIP on the electrode surface upon magneto-actuation (Videos S2 and S3). The magnetic-MIPs (0.55 mg) was incubated with L-thyroxine ranging from 3.8 × 10^{-6} to 388.4 μg mL^{-1} in citrate buffer (pH 7.0) for 30 min with gently shaking at 25 °C. The magnetic-MIP with the preconcentrated L-thyroxine was then magneto-actuated on the surface of the m-GEC electrode (Videos S2 and S3) for the electrochemical readout by linear sweep voltammetry (LSV) at 50.0 mV s^{-1} scan rate between 0.0 and 1.0 V vs. Ag/$AgCl/KCl_{(satd.)}$ reference electrode. All experiments were performed in a 0.1 mol L^{-1} HCl as supporting electrolyte. Before each use, the m-GEC electrode was cleaned by mechanical polishing and electrochemical treatment at a potential of +1.5 V for 4 s in 0.5 mol L^{-1} H_2SO_4.

3. Results and discussion

3.1. Theoretical study of L-thyroxine conformation

The initial geometry optimization of some neutral conformers of L-thyroxine was performed at the B97-D/def2-SV(P)/PCM level of theory, followed by frequency calculations. Fig. S3 (Supp. data) shows the most stable conformer for neutral L-thyroxine. Further discussion of this structure is provided in Supp. data, as well as the complete geometry (in cartesian coordinates) (Annex S1).

3.2. Theoretical study of the interactions of L-thyroxine with different monomers

The geometries of the neutral monomers and L-thyroxine were fully optimized using the B97-D/def2-SV(P) methodology. Afterwards, possible binding sites were thus proposed based on proton acceptors (oxygen and nitrogen atoms). The interactions between monomers and four different sites of L-thyroxine (amino, carboxylic, ether and hydroxyl groups, as shown in Fig. S3) were analyzed. The monomer/L-thyroxine complexes were studied taking into account the most stable conformational structure. Table 1 summarizes the energy values for the noncovalent binding of the 4:1 monomer/L-thyroxine complexes for each of the monomers considered, specifically the free energy ($\Delta G_{298.15\,K}$), the electronic energies (ΔE) and the enthalpy ($\Delta H_{0\,K}$). As shown in Table 1, and according to the thermodynamic values, the itaconic acid is the most suitable monomer, followed by methacrylic and acrylic acid. A previous report presented a MIP for the determination of L-thyroxine in blood serum samples synthesized with 1–3-diacroloylurea as functional monomer (Prasad et al., 2010). Nevertheless, the discussion of the thermodynamics aspects and/or the rational choice of the monomer were disregarded. The 1–3-diacroloylurea monomer presented a ΔG (0.4 kcal mol^{-1}) and ΔE (−64.6 kcal mol^{-1}) higher than itaconic acid (ΔG = −13.2 kcal mol^{-1}, ΔE = −70.8 kcal mol^{-1}). The lowest energy values for the itaconic acid were

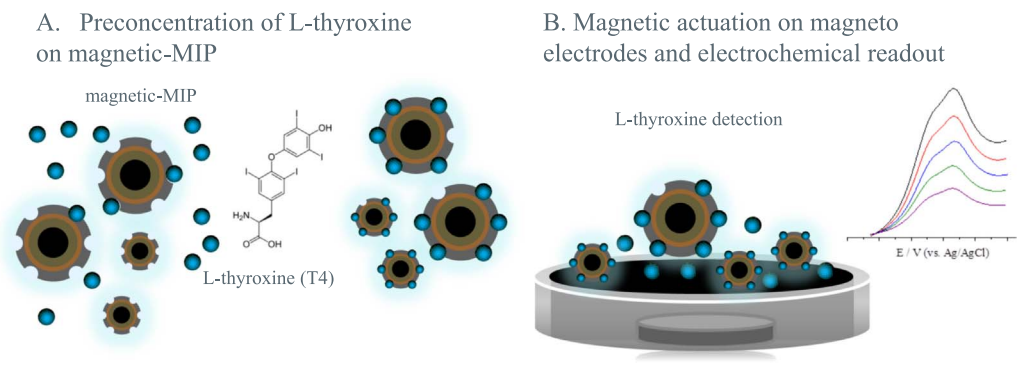

Fig. 2. Schematic procedure for the electrochemical sensing of L-thyroxine preconcentrated on magnetic-MIP on m-GEC electrodes.

expected, since this monomer contains two carboxylic groups, which favors the formation of more stable hydrogen bond interactions. These interactions have an important role in directionality, as further discussed in Supp. data. The optimized 3D model and Z-matrix for 4:1 itaconic/L-thyroxine complex is provided in the Fig. S4 and Annex S2 (Supp. data), respectively. Moreover, the optimized Z-matrices for all 4:1 monomers/L-thyroxine complexes are provided in the Annex S3 (Supp. data). Based on the high stability from values of ΔE, ΔH, ΔG and the high directionality of the multiple hydrogen bond interactions in the itaconic/L-thyroxine complex, further studies based on this complex

Table 1
Noncovalent binding free energy ($\Delta G_{298.15\,K}$), electronic energy (ΔE) and enthalpy ($\Delta H_{0\,K}$) for the 4:1 monomer/L-thyroxine complexes considering water as a solvent at B97-D/def2-SV(P)/PCM level.

Monomer	*Structure*	$\Delta G_{298.15\ K}$ *kcal mol*$^{-1}$	*ΔE*	$\Delta H_{0\,K}$
Itaconic acid	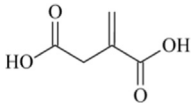	−13.3	−70.8	−65.6
Methacrylic acid	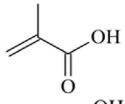	−10.1	−59.9	−55.2
Acrylic acid	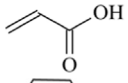	−8.6	−57.6	−52.8
4-Vinylpyridine	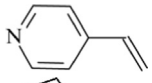	−7.6	−61.2	−56.9
1-Vinylimidazole	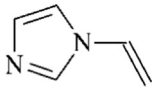	−4.5	−59.9	−55.1
Acrylamide	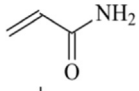	−0.4	−49.3	−44.3
Methacrylamide	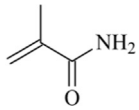	−0.4	−49.3	−44.3
1–3-diacroloylurea	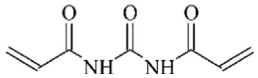	0.4	−64.6	−59.4
p-divinylbenzene	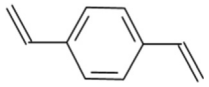	4.2	−52.8	−47.4
2-Vinylpyridine	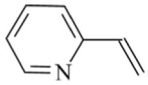	4.9	−45.2	−40.7
Methacrolein	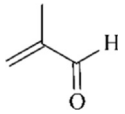	8.1	−42.1	−36.1
Acrolein	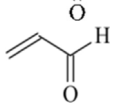	10.4	−37.1	−31.2
Acrylonitrile	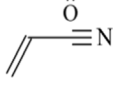	15.5	−31.8	−26.4

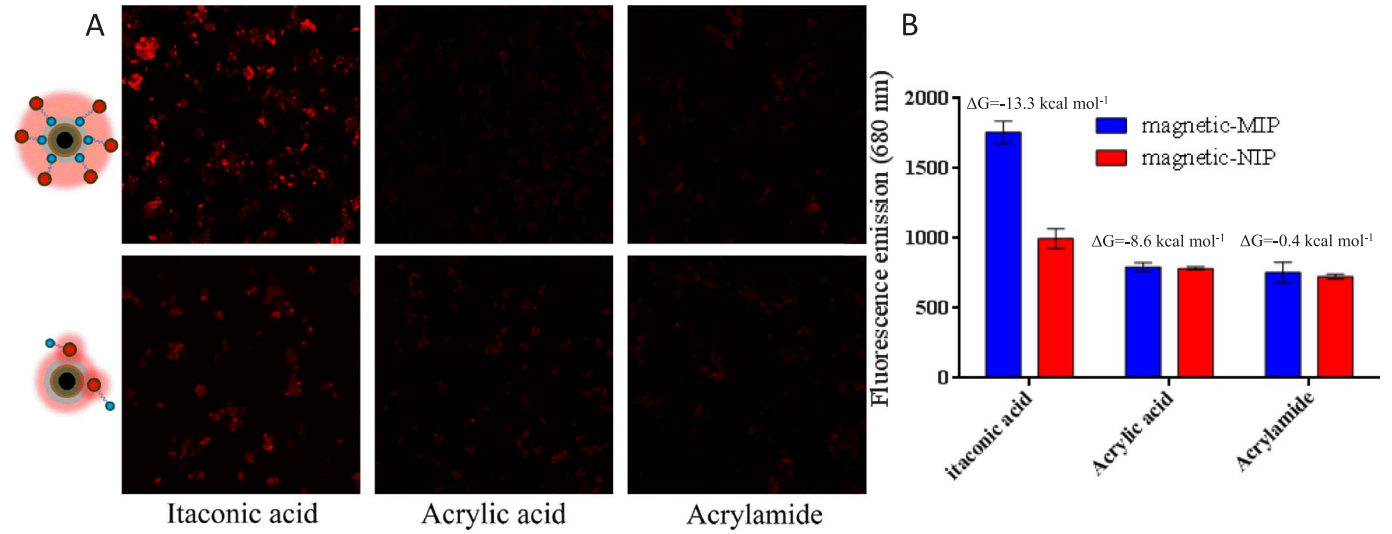

Fig. 3. (A) Characterization by laser confocal microscopy of the binding of T4-Atto665 conjugate (5.0 μmol L^{-1}) on the magnetic-MIPs and their corresponding NIPs synthesized with itaconic acid, acrylic acid and acrylamide. (B) Fluorescence emission intensity at 680 nm. The values for the noncovalent binding free energy ($\Delta G_{298.15\,K}$) related to each 4:1 monomer/L-thyroxine are also indicated in each case.

are presented in the next section.

3.3. Theoretical study of the monomer-monomer interactions

The monomer-monomer cooperativity is important to promote conformational changes, which most likely align specific structures between monomers, increasing the number of intermolecular interactions. In addition, the solvent effects on itaconic acid dimer was evaluated in n-hexane, benzene, toluene, ethanol and water solvents by PCM approach at the B97-D/def2-SV(P) level (Table S1, Supp. data). Further discussion is provided in Supp. data.

3.4. Theoretical study of the solvent effect

The polarity of the solvent could affect the conformation of the complex and the way that monomers recognize the template, altering the binding energy. The affinity of the itaconic/L-thyroxine complex was evaluated in different solvents (Skyner et al., 2015). Fig. S5 and Table S2 (Supp. data) summarizes the noncovalent binding free energy (ΔG) for 4:1 itaconic/L-thyroxine complex in the different implicit solvents. A spontaneous ΔG is observed for all solvents studied. However, the itaconic/L-thyroxine complex is less favored using polar solvents. To summarized, both n-hexane and benzene lead to a better stabilization of the complex, producing the weakest interference on itaconic/L-thyroxine interaction. Furthermore, the solvent molecule was explicitly included in positions involved in the hydrogen bonding. The system was modeled by using their respective dielectric continuum medium methodology (Polarizable Continuum Model, PCM). The itaconic acid and L-thyroxine interaction based on COOH groups was saturated by explicit n-hexane, benzene, toluene, ethanol and water molecules, separately. From Table S3 (Supp. data), the thermodynamic properties of n-hexane as solvent showed to be more suitable to prepare the magnetic-MIPs due to the nonspontaneous ΔG with itaconic acid (4.6 kcal mol^{-1}) and L-thyroxine (2.2 kcal mol^{-1}). The free energy for the binding of water as solvent to the itaconic acid monomer is highly spontaneous, leading to an undesired interaction competition. A complete discussion is provided in Supp. data.

3.5. Theoretical study of the stoichiometry

The study of itaconic/L-thyroxine interaction at different monomer ratios were performed at the same level of theory. A full discussion is provided in Supp. data (Fig. S6 and Table S4), while the optimized Z-matrices for all itaconic/L-thyroxine complexes are provided on Annex S4. The most efficient bonds are formed with the smaller complexes (1:1 and 2:1) to up to four monomers, while for larger complexes a quasi-stationary behavior is observed on average.

3.6. Synthesis and characterization of the magnetic molecularly imprinted polymers for L-thyroxine

The detailed core-shell synthesis is described in Supp. data (Schemes S3–S5), and summarized in Fig. 1. First of all, the magnetic core of Fe_3O_4 nanoparticles were evaluated by selected-area electron diffraction (Fig. S7 and Table S5), and by X-ray diffraction (Fig. S8, Supp. data). Furthermore, after each step of the core-shell synthesis, the products were collected and submitted to SEM, TEM and elemental analysis by Energy dispersive X-ray spectroscopy, and the results are presented in Figs. S9–S11 (Supp. data). The images revealed irregular spherical shape nanoparticles highly cross-linked among (Fig. S10). Moreover, the polymer includes many nanoparticles of magnetite in the structure, in agreement with the high magnetization of the material (Videos S1–S3, Supp. data). Finally, the template removal from the magnetic-MIP was confirmed by spectrophotometry (Fig. S12) and FTIR (Fig. S13, Supp. data). Further discussion of the characterization is provided in Supp. data.

3.7. Experimental evaluation of the performance of the magnetic-MIPs and magnetic-NIPs

In order to verify the predictive value of the theoretical calculations, three magnetic-MIPs (and magnetic-NIPs) based on different functional monomers (itaconic acid, acrylic acid and acrylamide) were synthesized. Although, the n-hexane and benzene lead to a better stabilization of the itaconic/L-thyroxine complex (Fig. S5), the L-thyroxine is poorly soluble in these solvents. Instead, ethanol, as an environmentally friendly solvent was used, while the stoichiometry of 4:1 monomer/template ratio was chosen (Fig. S6).

3.8. Laser confocal microscopy

The fluorescence patterns for the binding of T4-Atto655 on magnetic-MIPs (and magnetic-NIPs as a control for the specificity) performed with itaconic acid, acrylic acid and acrylamide, were evaluated

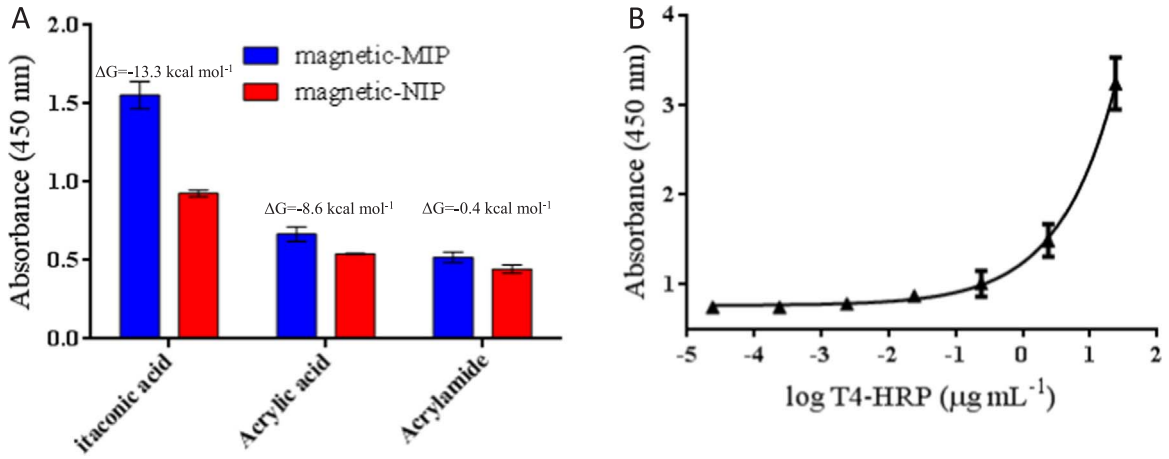

Fig. 4. (A) Characterization for the binding of 2.4 μg mL^{-1} T4-HRP conjugate by magneto-immunoassay on the magnetic-MIPs and their corresponding NIPs synthesized with itaconic acid, acrylic acid and acrylamide as functional monomers. (B) Calibration plot for T4-HRP conjugate in concentration range from 2.40 × 10^{-4} to 24.00 μg mL^{-1}. The negative control (0 μg mL^{-1} T4-HRP) is also shown. Error bar illustrates the standard deviation (n = 3).

by laser confocal microscopy, as schematically described in Fig. S1 (Supp. data). The Fig. 3, panel A shows the binding patterns while Fig. 3, panel B presents the quantitative emission intensity data taken from three different images (n = 3).

As shown in Fig. 3, the highest fluorescence is observed for the magnetic-MIP synthesized with itaconic acid, while in the case of the acrylic acid and acrylamide the fluorescence is almost negligible, and similar to that of the magnetic-NIP for itaconic acid synthesized without the L-thyroxine as a template. The small fluorescence observed can be attributed to the porosity of this materials, since the small-sized T4-Atto655 conjugate can thus freely enter in some cavities of the polymer. Accordingly to the results, the theoretical calculations successfully demonstrate a good prediction for the binding of L-thyroxine-Atto655 conjugate on the magnetic-MIP.

3.9. Magneto-actuated immunoassay

The binding of L-thyroxine conjugated to the enzyme horseradish peroxidase (T4-HRP) on magnetic-MIPs and magnetic-NIPs were evaluated by magneto-actuated immunoassay, as schematically described in Fig. S2 (Supp. data). As it is shown in Fig. 4, panel A, the binding efficiency of T4-HRP conjugate on the magnetic-MIP synthesized with itaconic acid was considerably higher than acrylic acid and acrylamide as functional monomers, in agreement with the laser confocal microscopy. A complete calibration plot is shown in Fig. S14 (Supp. data) for all the concentration range (2.40 × 10^{-4} to 24.00 μg mL^{-1}). It is important to highlight that these experimental results are again in agreement with the theoretical calculations in order to predict *in silico* the functional monomer with better binding performance, demonstrating a reliable way in the rational MIP design. The influence in the binding of buffer of different composition and pH (Table S6, Supp. data) was also studied for itaconic acid magnetic-MIP and NIP (Fig. S15, Supp. data). The better binding performance was achieved by using citrate buffer pH = 7, in agreement with previous studies (Ben Aissa et al., 2016).

Fig. 4, panel B shows the calibration plot for the detection of T4-HRP by the magneto-actuated immunoassay using magnetic-MIP synthesized with itaconic acid as functional monomer, in concentration range from 2.40 × 10^{-4} to 24.00 μg mL^{-1}. The results were fitted (R^2 = 0.9827) to a four-parameter logistic equation (sigmoidal dose-response/variable slope). The limit of detection (LOD) was estimated by processing the negative control (n = 11), but omitting the addition of T4-HRP (0 μg mL^{-1}). The cut-off value was calculated then determined with a one-tailed *t*-test (t = 1.812) at a 95% confidence level, giving a value of 0.866 AU. The LOD was found by interpolation of this value, being as low as 0.048 μg mL^{-1} T4-HRP.

3.10. Electrochemical sensing on magneto-actuated electrodes

The previous result showed the binding performance of L-thyroxine conjugated to an enzyme (HRP) or dye (Atto655) and using different readouts in order to experimentally evaluate the prediction capacity of the theoretical model. The conjugation was performed by activation of the free COOH group of the L-thyroxine activated by NHS/DCC for conjugation to amino groups of HRP and amine-Atto655, as shown in Schemes S1 and S2 (Supp. data). However, the magnetic-MIP was synthesized with non-conjugated L-thyroxine molecule, in which all the functional groups of L-thyroxine were available for non-covalent binding with the monomer. This fact involves as a main drawback the non-perfect matching of L-thyroxine in the magnetic-MIPs cavities, due to the lack of free COOH group. Moreover, the enzymatic or fluorescent tag can prevent by steric hindrance the occupancy of all the binding cavities of the MIPs and produce non-specific adsorption. Since the L-thyroxine is electroactive (Fig. S16, Supp data), the direct electrochemical detection of L-thyroxine preconcentrated on 0.55 mg the magnetic-MIP by magnetic actuation on m-GEC electrodes was performed for the first time, as schematically shown in Fig. 2. First of all, the optimization of the amount of magnetic-MIP was performed by SEM, by changing the amount of the surface of the electrode from 0.10; 0.55 (Video S2) and 1.00 mg (Video S3). As observed in Fig S17 (Supp. data), the amount of 0.55 is enough to provide a full coverage of the surface of the electrode as a monolayer but leaving bare zones in order to achieve the direct electron transfer of L-thyroxine on the m-GEC electrode. Higher amount of material produced clumping of the magnetic-MIP (Video S3), which can prevent the electrochemical detection of the L-thyroxine since not bare zones of the electrodes were observed.

Fig. 5, panel A shows comparatively the anodic current values at +0.90 V (corrected by base line) of the LSV for detection of the L-thyroxine onto magnetic-MIPs and the corresponding magnetic-NIPs performed with itaconic acid, acrylic acid and acrylamide as functional monomers. As expected, the magnetic-MIP synthesized with itaconic acid as functional monomer shows the higher current peak at 0.90 V vs. Ag/AgCl, while the magnetic-NIP shows a negligible current peak (Fig. S18, Supp. data).

Moreover, it is important to highlight the preconcentration of L-thyroxine provided by the magnetic MIP. By comparing the magneto-actuated electrode covered with the magnetic-MIP (Fig. S18) and the bare electrode (Fig. S16), at the same concentration of L-thyroxine, the electrochemical signal is much higher in the case of the electrochemical sensing based on the magnetic-MIP. Beside the increased sensitivity, the

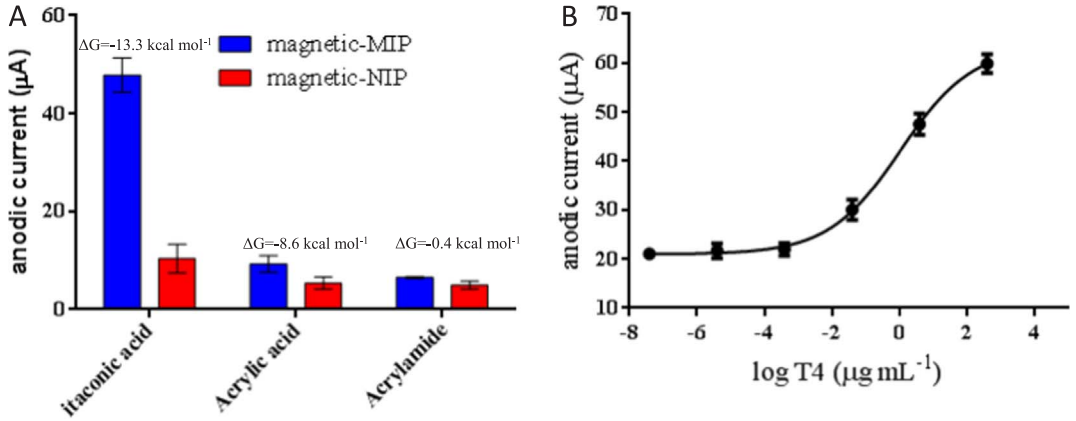

Fig. 5. (A) Current signal at 0.90 V of 3.88 μg mL^{-1} L-thyroxine preconcentrated onto magnetic-MIPs and magnetic-NIPs synthesized with itaconic acid, acrylic acid and acrylamide as the functional monomers. (B) Calibration plot for the electrochemical sensing of L-thyroxine in concentration ranging from 3.88 × 10^{-6} to 388.4 μg mL^{-1}. The negative control (0 μg mL^{-1} T4) is also shown. Error bar illustrates the standard deviation for the samples (n = 3). Supporting electrolyte 0.10 mol L^{-1} HCl, 50.0 mV s^{-1} scan rate.

magnetic-MIP provides further specificity when tested together with common serum metabolites, such as uric and ascorbic acid, glucose and dopamine, as discussed in Fig. S19, Supp. data. After separation on the magnetic-MIP, only the anodic signal corresponding to L-thyroxine is observed (panel E), while the signal corresponding to uric acid at 0.759 V (panel F) is eliminated due to the specificity of the magnetic-MIP. Finally, a calibration plot based on the anodic current peak values at 0.9 V for L-thyroxine was obtained by LSV, using magnetic-MIP synthesized with itaconic acid as functional monomer (Fig. 5, panel B) in concentration ranging from 3.88 × 10^{-6} to 388.4 μg mL^{-1}. The results were fitted (R^2 = 0.9908) to a four-parameter logistic equation. The limit of detection (LOD) was estimated by processing the negative control (n = 4), but omitting the addition of T4 (0 μg mL^{-1}). The cut-off value was then determined with a one-tailed *t*-test (t = 2.132) at a 95% confidence level, giving a value of 21.59 μA. The LOD was found by interpolation of this value, being as low as 0.0356 ng mL^{-1}, much lower than the values for the normal euthyroid adult population, ranging from 50 to 125 ng mL^{-1} for total thyroxine (although it is recommended that each laboratory establish the own normal range, which may be unique to the population depending upon geographical, patient, dietary, or environmental factors). As previously discussed, the detection of total T4 is mostly performed by competitive immunoassay, in which a 96-well plate is precoated with anti-Thyroxine antibodies. Samples and the thyroxine (T4)-HRP conjugate are added to the wells, where thyroxine in the sample competes with the added Thyroxine-HRP conjugate for antibody binding. Table S7 summarized the main analytical performance (including principle, normal range, LOD and assay time) of total T4 Commercial Kit from six companies, including Abcam (UK, Product No. ab178664), Invitrogen ThermoFisher (USA, Product No. EIAT4C), IBL international (Germany, Product No. RE55261) and MP Biomedicals (USA, Product No. 07BC-1007). Moreover, two automated procedures based on the more sensitive chemiluminescent readout were also including: Abbott (Germany, Product No. B7K660) and Beckman Coulter (USA). It is important to highlight that the last one is based on a magneto-actuated immunoassay using microparticles recovered with specific antibodies. In all cases, the LOD obtained with the electrochemical sensor was much lower than those reported by the commercial kits involving also longer total assay times, even in the case of chemiluminescent readout in the automated procedure based on magnetic particles.

4. Conclusions

The *in silico* quantum chemistry calculations based on DFT-D methodology showed to be a useful and reliable tool for the rational MIP design with an impressive predictive value, including selection of functional monomer, solvent effects and stoichiometry. The theoretical results were experimentally confirmed by comparing the binding performance of three different functional monomers. Higher binding capacity and selectivity was achieved for the magnetic-MIP synthesized with itaconic acid, as theoretically predicted. The magnetic-MIP shows remarkable features, including long-term storage at room temperature, low cost and animal-free production, offering an exciting alternative for replacing the L-thyroxine antibodies in the gold standard methods. Beside this, as it was demonstrated in this work, the material is compatible with optical, fluorescent and electrochemical readout. Finally, the direct electrochemical sensing of thyroxine preconcentrated on the magnetic-MIP in magneto-actuated electrodes is also described for the first time, showing promising analytical performance, including simplicity in the procedure, assay time (30 min) and LOD (as low as 0.0356 ng mL^{-1} which cover the clinical range of total L-thyroxine). A good selectivity was also demonstrated in synthetic samples spiked with for common serum metabolites. Future work will be focused on the quantification of the hormone in biological specimens including serum, EDTA and heparin plasma and urine.

Acknowledgments

Ministry of Economy and Competitiveness (MINECO), Madrid (Grant BIO2016-75751-R), Fundação de Amparo à Pesquisa do Estado de São Paulo (Grants 2017/07707-3, 2014/25264-3, and 2014/50945-4), and Conselho Nacional de Desenvolvimento Científico e Tecnológico, Ministry of Science, Technology and Innovation of Brazil (Grants 307052/2016-8, 404337/2016-3, 309051/2016-9, 406107/2016-5, 233595/2014-7 and 465571/2014-0) are gratefully acknowledged.

Appendix A. Supporting information

Supplementary data associated with this article can be found in the online version at http://dx.doi.org/10.1016/j.bios.2018.01.028.

References

Antony, J., Grimme, S., 2006. Phys. Chem. Chem. Phys. 8, 5287–5293.
Ben Aissa, A., Herrera-Chacon, A., Pupin, R.R., Sotomayor, M.D.P.T., Pividori, M.I., 2016. Biosens. Bioelectron. 88, 101–108.
Bhaskarapillai, A., Chandra, S., Sevilimedu, N.V., Sellergren, B., 2009. Biosens. Bioelectron. 25, 558–562.
Dayan, C.M., 2001. Lancet 357, 619–624.
Frisch, M.J., Trucks, G.W., et al., 2013. Gaussian 09 Revision D.01.
Gentile, F., DiLauro, R., Salvatore, G., 1995. Biosynthesis and secretion of thyroid hormones. In: DeGroot, L.J. (Ed.), Endocrinology. WB Saunders Company, Philadelphia, pp. 517–542.
Grimme, S., 2006. J. Comput. Chem. 27, 1787–1799.

Hay, P.J., Wadt, W.R., 1985. J. Chem. Phys. 82, 299–310.
Huynh, T.-P., Kutner, W., 2015. Biosens. Bioelectron. 74, 856–864.
Jolly, P., Tamboli, V., Harniman, R.L., Estrela, P., Allender, C.J., Bowen, J.L., 2016. Biosens. Bioelectron. 75, 188–195.
Mahon, C.S., Fulton, D.A., 2014. Nat. Chem. 6, 665–672.
Midgley, J.E., 2001. Clin. Chem. 47, 1353–1363.
Nicholls, I.A., Andersson, H.S., Charlton, C., Henschel, H., Karlsson, B.C.G., Karlsson, J.G., O'Mahony, J., Rosengren, A.M., Rosengren, K.J., Wikman, S., 2009. Biosens. Bioelectron. 25, 543–552.
Pividori, M.I., Alegret, S., 2005. Anal. Lett. 38, 2541–2565.
Prasad, B.B., Madhuri, R., Tiwari, M.P., Sharma, P.S., 2010. Anal. Chim. Acta 681, 16–26.
Ren, X., Chen, L., 2015. Biosens. Bioelectron. 64, 182–188.
Řezáč, J., Hobza, P., 2016. Chem. Rev. 116, 5038–5071.
Rosengren, A.M., Golker, K., Karlsson, J.G., Nicholls, I.A., 2009. Biosens. Bioelectron. 25, 553–557.
Scalmani, G., Frisch, M.J., 2010. J. Chem. Phys. 132, 114110–114125.
Skyner, R.E., McDonagh, J.L., Groom, C.R., Van, M.T., Mitchell, J.B.O., 2015. Phys. Chem. Chem. Phys. 17, 6174–6191.
Vlatakis, G., Andersson, L.I., Müller, R., Mosbach, K., 1993. Nature 361, 645–647.
Wang, D., Gan, N., Zhang, H., Li, T., Qiao, L., Cao, Y., Su, X., Jiang, S., 2015. Biosens. Bioelectron. 65, 78–82.
Weigend, F., Ahlrichs, R., Peterson, K.A., Dunning, T.H., Pitzer, R.M., Bergner, A., 2005. Phys. Chem. Chem. Phys. 7, 3297–3305.
Zeng, Y., Zhou, Y., Kong, L., Zhou, T., Shi, G., 2013. Biosens. Bioelectron. 45, 25–33.